

# Observing Precipitation through Dual-Polarization Radar Measurements

Paul H. Herzegh\*  
and Arthur R. Jameson†

## Abstract

Dual-polarization radar measurements of precipitation are primarily influenced by the size, shape, orientation, and phase of scattering hydrometeors. As a result, these measurements can serve as a tool for remote identification of hydrometeor characteristics.

This paper presents an overview of the definitions, observed values, and applications of differential reflectivity ( $Z_{DR}$ ) and linear depolarization ratio (LDR) measurements. Brief examples of these measurements are given for widespread stratiform precipitation, a rapidly developing convective cell, and a severe hailstorm. The results outline the role that  $Z_{DR}$  can play in the differentiation of rain and solid precipitation, identification of supercooled raindrops above the 0°C level, and identification of hail at the surface. LDR measurements are seen to reveal contrasts in ice-particle shape, orientation, and particle phase. These contrasts are of particular benefit toward delineation of hail regions aloft and identification of mixed-phase particle growth environments.

## 1. Introduction

Meteorological radars use information conveyed by the amplitude, phase, wavelength, and polarization of backscattered electromagnetic waves. Applications such as conventional weather surveillance generally use only amplitude data obtained at a single, fixed polarization to derive a measure of radar reflectivity and precipitation intensity. In this application, horizontal polarization (in which the electric vector of the transmitted wave oscillates in the horizontal plane) is typically used. By transmitting and/or receiving radar signals in two orthogonal polarization states, however, dual-polarization radars can obtain more detailed information related specifically to the size, shape, orientation, density, and thermodynamic phase of precipitation particles. This information can lead to inferences previously obtainable only by in situ observations from airborne or ground-based facilities. Applications of dual-polarization radar in operations and research include rainfall measurement (Seliga and Bringi

1976; Hall et al. 1980; Seliga et al. 1981; Ulbrich and Atlas 1984), hail detection (Bringi et al. 1984, 1986; Aydin et al. 1986; Illingworth et al. 1986) and identification of hydrometeor types (Hall et al. 1984; Hendry and Antar 1984; Liu and Herzegh 1986; Bader et al. 1987; Illingworth et al. 1987; Illingworth 1988). Very useful discussions of each of these topics can also be found in Atlas (1990).

Most of the work cited above has centered on the use of linear polarizations, in which the transmitted wave is plane polarized (e.g., horizontal or vertical polarization). At these polarizations, extensive use has been made of copolar power measurements, in which backscattered radar returns are measured in the same polarization as that transmitted. The shapes and spatial orientations of hydrometeors, however, also induce some of the transmitted wave at one polarization (say, horizontal) to return to the radar with the orthogonal (vertical) polarization. Thus, additional meteorological information can often be obtained by examination of cross-polar measurements.

In this paper we present an overview of linear copolar and cross-polar radar measurements in a variety of meteorological situations, and we outline some of the opportunities for application of these measurements to the study of precipitation. Although a number of techniques using signal correlation (Illingworth and Caylor 1988), phase relationships (Sachidananda and Zrnić 1986), and coherent radar (Metcalf 1986) show excellent potential, we limit our overview to direct interpretation of simple copolar and cross-polar power measurements.

## 2. Polarization radar parameters

The variety of dual-polarization data types currently measured stems from the number of options available for transmitting a radar wave and receiving the backscattered returns. For current meteorological applications, the polarization state of the transmitted pulse is typically either linear or circular, in which the orientation of the electric vector rotates continuously through 360° at the radar frequency, while its magnitude is constant. In either case, it is desirable to record

\*National Center for Atmospheric Research, Boulder, Colorado. (The National Center for Atmospheric Research is sponsored by the National Science Foundation.)

†Applied Research Corporation, Landover, Maryland.  
©1992 American Meteorological Society

both the copolar and cross-polar components of the returned signal.

The parameters discussed in this section are generally obtained directly from linear polarization measurements. Jameson (1987) and Jameson and Davé (1988), however, show that parameters such as these can also be derived from circular polarization measurements.

#### a. Differential reflectivity

During their fall to earth, raindrops larger than 1–2 mm in diameter are deformed into oblate spheroids by aerodynamic forces (Pruppacher and Beard 1970). Though some slight disturbance in their orientation may be induced by turbulence, drop collisions, and aerodynamic instability, the drops fall with their maximum dimensions oriented in the horizontal. Consequently, scattering and propagation will differ for horizontally and vertically polarized radar waves. For example, in moderate to heavy rain the radar reflectivity at horizontal polarization ( $Z_h$ , in dBZ) tends to be slightly stronger than that at vertical polarization ( $Z_v$ , in dBZ). Differential reflectivity ( $Z_{DR}$ ) is a measure of that difference and is equivalent to the quantity  $Z_h$  minus  $Z_v$ . Here  $Z_{DR}$  is expressed in decibels (dB), with values of 0 to ~ 5 dB being typical of rain. In practice, the  $Z_h$  and  $Z_v$  measurements necessary to derive  $Z_{DR}$  can be most simply obtained using a single-channel radar capable of rapid switching between horizontal and vertical polarization. Depending upon the radar, switching may occur following transmission and reception of individual pulses or groups of up to several hundred pulses.

The magnitude of  $Z_{DR}$  in rain provides an indicator of mean drop shape (specifically, the reflectivity-weighted mean axis ratio; Jameson 1983). Because large raindrops deform to more extreme oblate shapes than smaller drops,  $Z_{DR}$  measurements can in turn be used to estimate mean drop size and (assuming a given drop spectrum shape) rainfall rate. For example, Fig. 1 gives the relation between  $Z_{DR}$  and raindrop diameter for individual drops [based on the drop-size shape relationship of Beard and Chuang (1987), and assuming that drop diameter is a small fraction of the radar wavelength].

The response of  $Z_{DR}$  to hydrometeor shape for ice differs greatly from that for water drops. Not only are the shapes of ice particles and water drops quite different, but  $Z_{DR}$  sensitivity to hydrometeor shape varies with the dielectric constant of the scattering particles. Since the effective dielectric constant of solid ice is about 20% that of water, particle shape has a much smaller effect on  $Z_{DR}$  measurements in ice than in liquid hydrometeors. The inclusion of air in ice particles of low bulk density, such as loose aggre-

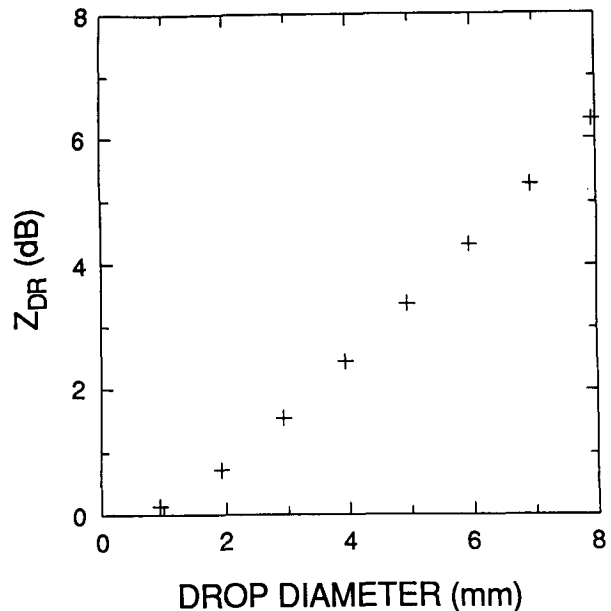


FIG. 1. Calculations of  $Z_{DR}$  in decibels as a function of drop diameter for the drop-size shape relationship of Beard and Chuang (1987). Calculations use the scattering theory of Gans (1912).

gates, lowers the effective dielectric constant further. In the case of aggregates, the ice–air mixture may be as low as 5%–10%. Thus,  $Z_{DR}$  sensitivity to the shapes of aggregate particles is generally very low.

The relationships between  $Z_{DR}$  and hydrometeor shape for uniform ice particles of various types are shown in Fig. 2. The relationships assume that the ice particles are oblate in shape and are oriented with their long axes in the horizontal. These curves were calculated according to the scattering theory of Gans (1912) and apply to raindrops, solid ice, graupel (density 0.3 to 0.6 g cm<sup>-3</sup>), and aggregate snow (density 0.03 to 0.12 g cm<sup>-3</sup>). Figure 2 shows that  $Z_{DR}$  is much less sensitive to particle shape for ice than for water.

The sensitivity of  $Z_{DR}$  measurements to particle shape (whether ice or liquid) also diminishes as the orientation of the particles becomes more random. Raindrops may cant up to several tens of degrees due to extreme wind shear, drop collisions (Johnson and Beard 1984) or drop breakup. Theoretical studies (Beard and Jameson 1983) and radar measurements (McCormick and Hendry 1974; Hendry et al. 1987), however, indicate that raindrop canting angles tend to be narrowly distributed about a mean value of zero. As a result, the influence of raindrop canting on  $Z_{DR}$  is generally slight. In contrast, icy hydrometeors exhibit considerably greater canting than raindrops, resulting in  $Z_{DR}$  values that are correspondingly closer to zero. The greater canting in icy hydrometeors is easily recognized in their tendency to wobble and spin during descent (e.g., Jayaweera and Mason 1965; Jayaweera

and Cottis 1969; Podzimek 1965, 1968; List and Schemenauer 1971; List et al. 1973; Zikmunda and Vali 1972). Canting is most pronounced in the larger and more compact icy hydrometeors (Jameson 1985), such as lumpy graupel or hail, which are known to tumble during fall (Knight and Knight 1970; List et al. 1973).

### b. Linear depolarization ratio

For linearly polarized radar transmissions, most of the energy scattered by interaction with hydrometeors retains the polarization of the incident wave. However, when nonspherical hydrometeors are present and are canted with respect to the axis of polarization (say, horizontal), a small fraction of the incident energy is depolarized, that is, scattered at the orthogonal polarization (vertical). The magnitude of this "small" fraction (typically 0.1% to 1%) depends upon the size and dielectric constant of the scatterers, their effective aspect ratio, their degree of canting, and the radar view angle.

The linear depolarization ratio (LDR) provides a measure of depolarization. For transmitted waves of linear horizontal polarization, LDR is given by the ratio of the depolarized return (which reaches the radar as a vertically polarized wave) over the copolar return

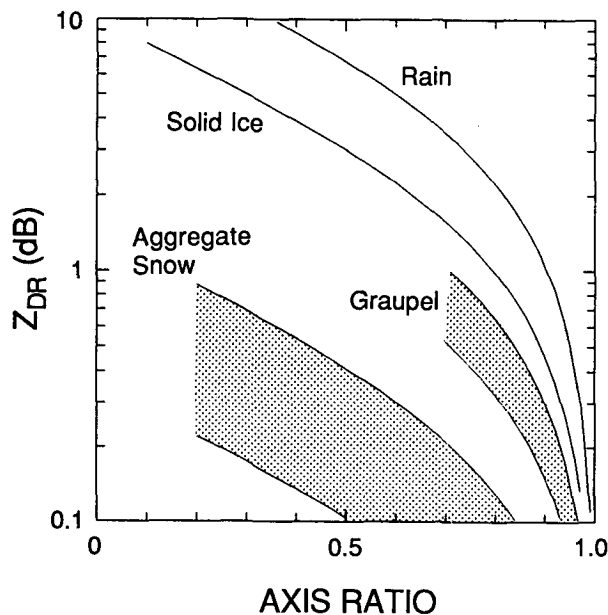


FIG. 2. Calculations of  $Z_{DR}$  in decibels as a function of particle axis ratio for spheroids having the effective dielectric properties of raindrops, solid ice, graupel, and aggregate snow. As axis ratio decreases from 1 toward 0, particle (spheroid) shape becomes more oblate. Curves shown for graupel cover bulk densities of  $0.3 \text{ g cm}^{-3}$  (lower boundary of shaded region) to  $0.6 \text{ g cm}^{-3}$  (upper boundary). Values shown for aggregate snow cover bulk densities of  $0.03 \text{ g cm}^{-3}$  (lower boundary of shaded region) to  $0.12 \text{ g cm}^{-3}$  (upper boundary). Calculations use the scattering theory of Gans (1912).

(which retains the horizontal polarization of the original transmitted wave). LDR is generally expressed in dB. Like  $Z_{DR}$ , the response of LDR to particle shape and canting effects is strongly tied to the effective dielectric constant of the scatterers. Thus, as we shall see in section 3, hydrometeors in mixed-phase or wetted conditions yield high-LDR signatures.

### c. Propagation effects for $Z_{DR}$ and LDR

It is important to note that the interaction between a radar wave and the hydrometeors it encounters can significantly modify the wave as it travels. Both the absorption and scattering of wave energy play a role in these propagation effects. The interpretation of dual-polarization radar measurements can at times be significantly compromised by these effects, particularly for shorter radar wavelengths. For example, the oblate shapes of raindrops can induce differential attenuation, in which attenuation at horizontal polarization is greater than that at vertical polarization. The anisotropic nature of rain or oriented ice-phase precipitation may also induce differential phase shift, in which return of the horizontal signal slightly lags that of the vertical signal, due to a slight difference in the propagation speeds at the two polarizations. Both are cumulative effects that, if present, progressively influence the radar measurements as the path length through the precipitation increases.

At wavelengths normally used for meteorological radars, only differential attenuation has a significant effect on  $Z_{DR}$  measurements. The influence is generally limited to wavelengths of  $\sim 5 \text{ cm}$  or less, where attenuation can be a significant problem in heavy precipitation. Differential attenuation tends to reduce radar estimates of  $Z_h$  more than  $Z_v$ , leading to  $Z_{DR}$  values that are biased toward zero. Since the  $Z_{DR}$  data presented in this paper were obtained at 10-cm wavelength, which is largely unaffected by attenuation in rain, differential attenuation is unlikely to have a significant effect upon  $Z_{DR}$ .

In contrast to  $Z_{DR}$ , LDR can be significantly affected by both of the propagation effects mentioned above. Measurements of LDR at 3.2-cm wavelength (such as described in section 3) are subject to serious contamination by differential attenuation in rain. For radars that transmit at horizontal polarization, differential attenuation leads to overestimates of LDR for path lengths greater than 5–10 km in rainfall of 5–10  $\text{mm h}^{-1}$  or more. Of course, the magnitude of the overestimate increases as rainfall rate and path length increase.

Differential phase shift can influence LDR measurements by progressively altering the polarization of the radar signal. Normally, as a horizontally polarized radar wave propagates through precipitation, it is

modified slightly by the forward-scattered contribution of the hydrometeors. Since some of the forward-scattered energy will be vertically polarized, the propagating wave can acquire a significant cross-polarized (vertical) component. As the component increases in magnitude, and differential phase shift causes the horizontal component to increasingly lag the vertical, the wave becomes elliptically polarized. This gradual transition from linear to elliptical polarization results in an increase in the downstream strength of the (apparent) depolarized power detected by the radar, and thus yields a misleading increase in measured values of LDR. Though more severe at the shorter wavelengths, differential phase shift can occur even at 10-cm wavelength (Humphries 1974).

In many situations, the cumulative impact of propagation effects can be easily recognized, and the impact can often be removed (or reduced in magnitude) through subsequent processing. In section 3d we present LDR observations after correction to mitigate propagation effects induced by heavy rain and hail in a convective storm. While the details of the correction technique are not important here, we do note that the technique is a direct outgrowth of that used by Jameson and Heymsfield (1980) to correct for attenuation of X-band radar measurements used in dual-wavelength hail studies.

### 3. Overview of dual-polarization radar observations

In this section we outline brief examples of dual-polarization radar observations obtained in stratiform and convective precipitation systems. Unless otherwise noted, the observations were obtained using the National Center for Atmospheric Research dual-wavelength CP-2 radar, which provides measurements of reflectivity,  $Z_{DR}$ , and Doppler velocity spectrum parameters at 10.7-cm wavelength (S-band), as well as reflectivity and LDR at 3.2-cm wavelength (X-band). The antennas at both wavelengths yield pencil beams of  $\sim 0.93^\circ$  beamwidth. Keeler et al. (1989) provide a comprehensive description of the CP-2 radar.

#### a. Stratiform ice-phase precipitation

Figure 3 presents CP-2 measurements along a vertical section at  $320^\circ$  azimuth through a region of widespread stratiform precipitation observed near Boulder, Colorado, on 24 May 1984. In Fig. 3a, a well-defined radar bright band associated with hydrometeor melting appears at 2 km above ground level (AGL), beneath a  $Z_h$  field that shows the remnants of weak embedded convection. The strength of the bright band indicates that the precipitation above is com-

prised mainly of low-density ice particles such as aggregates (see review of brightband interpretation in Battan 1973). Blocking of the radar beam by mountain peaks prevents low-level radar observations past the 12-km range.

The most prominent feature in Fig. 3b is the  $Z_{DR}$  bright band at 1.5 to 2 km AGL. This band marks the presence of transitional, horizontally aligned ice-water particle structures formed during the melting of snow. Below the  $Z_{DR}$  bright band, further melting causes the structures to collapse to more spherical forms, leading to a rapid decrease in  $Z_{DR}$ . The low values of  $Z_h$  and the near-zero values of  $Z_{DR}$  in the rain region are indicative of drizzle.

Here,  $Z_{DR}$  is nearly structureless in the snow above 2 km AGL in Fig. 3b and fluctuates slightly around a mean value of 0.0 to 0.2 dB. The fluctuations are due to random variance or "noise" in the radar estimates of  $Z_h$  and  $Z_v$ . The near-zero values of  $Z_{DR}$  shown are characteristic of low-density aggregate forms and result from the quasi-spherical shapes of aggregates and the reduced sensitivity of  $Z_{DR}$  to shape effects in low-density ice (section 2a). Only dense, highly aspherical forms (such as single-crystal snow) falling in a highly oriented manner can be expected to yield  $Z_{DR}$  values that are significantly higher, in the 1- to 3-dB range. The higher values of ZDR shown near cloud top in Fig. 3b are artifacts resulting from CP-2 beam pattern effects rather than particle shape. These effects are discussed by Herzegh and Carbone (1984), who show that certain  $Z_{DR}$  signatures suggestive of marked changes in ice-particle type in reflectivity gradient regions can result from mismatch in the antenna beam patterns at horizontal and vertical polarization.

Although the present example depicts a relatively uniform field of  $Z_{DR}$ , several investigators (Hall et al. 1984; Bader et al. 1987) have reported  $Z_{DR}$  measurements that indicate considerable structure in stratiform precipitation. These studies suggest that  $Z_{DR}$  can be a useful indicator of certain contrasts in particle structure. Liu and Herzegh (1986), however, present striking observations of  $Z_{DR}$  structure in stratiform precipitation that are shown through in situ measurements to be unrelated to changes in particle type. In these cases, beam-pattern mismatch effects caused the observed  $Z_{DR}$  signatures. Thus, application of  $Z_{DR}$  measurements to the study of precipitation structure must be carried out only with a full understanding of the influence of antenna beam patterns at horizontal and vertical polarization.

LDR measurements along the same vertical section are shown in Fig. 3c. Since the cross-polar returns are generally very weak, LDR coverage is often limited to regions of relatively high reflectivity and/or regions

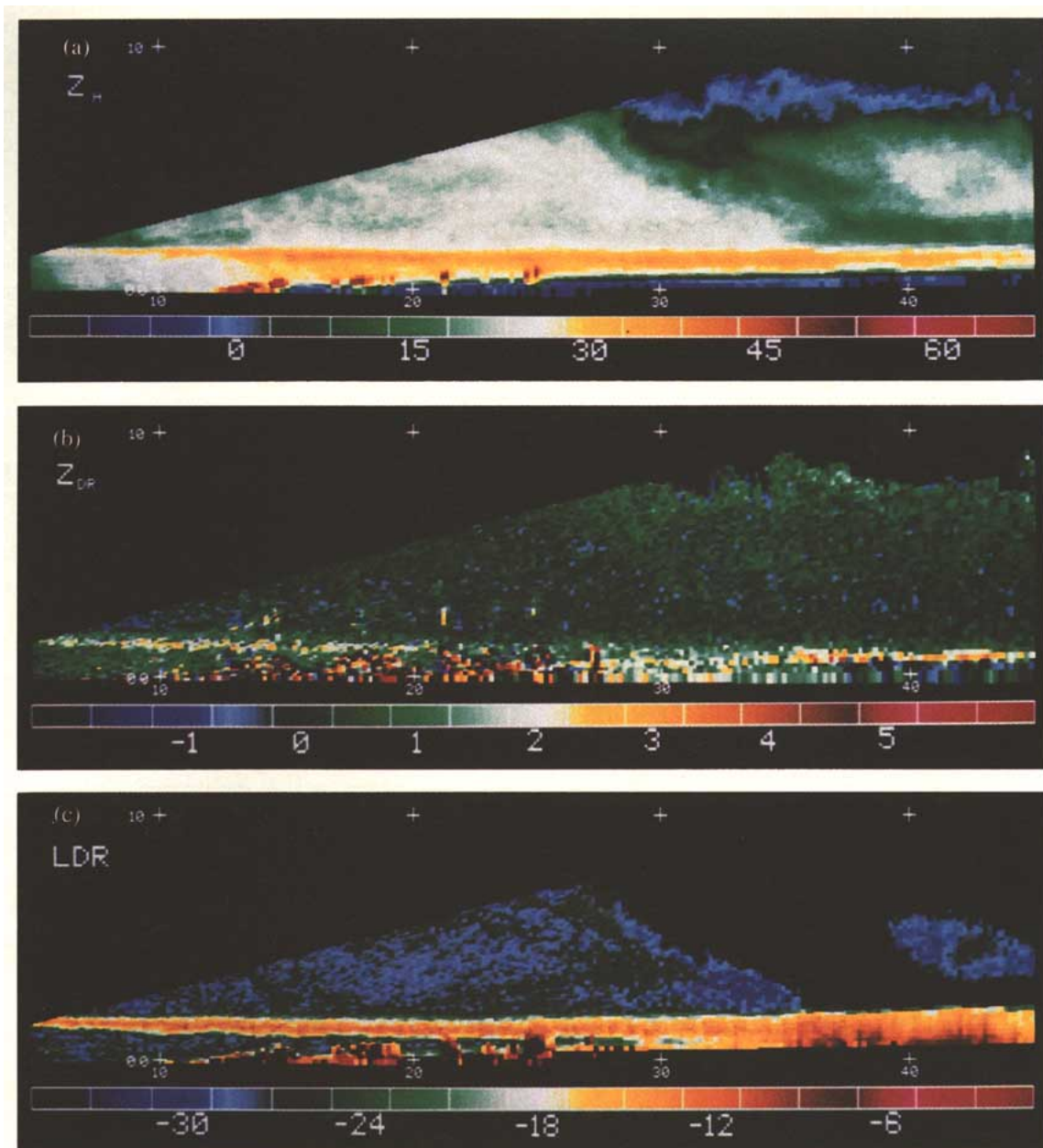


FIG. 3. CP-2 radar data for a vertical section through stratiform upslope precipitation observed on 24 May 1984 near Boulder, Colorado. Color scales at bottom of (a), (b), and (c) indicate values of  $Z_h$ ,  $Z_{DR}$ , and LDR, respectively. (a)  $Z_h$  (dBZ) showing a well-defined melting-level bright band at 2 km AGL. (b)  $Z_{DR}$  (dB) showing a  $Z_{DR}$  bright band near 2 km AGL. (c) LDR (dB) showing a LDR bright band near 2 km AGL. Regions in which LDR signals are below the detectable level are shown in black.

close to the radar. This restriction can be easily seen for the present example in Fig. 3c.

The measured values of LDR shown in the snow region in Fig. 3c are quite low (approximately  $-26$  to  $-29$  dB), and are typical of stratiform growth environments lacking mixed-phase precipitation particles. As outlined in section 2b, the response of LDR to particle shape and canting effects increases dramatically for particles having a high effective dielectric constant, such as liquid or mixed-phase hydrometeors. The

response to irregularly shaped mixed-phase particles can be seen in the high LDR values observed in the melting region ( $\sim 2$  km AGL). Here, asymmetrical, partially melted aggregates with ill-defined orientations result in a striking increase in LDR, which reaches peak values of  $-14$  to  $-10$  dB to form an "LDR bright band." In the drizzle below the melting region, LDR abruptly returns to low values ( $-26$  to  $-29$  dB), which are consistent with submillimeter-size drops showing little oblate deformation or canting.

### *b. Rapidly developing convective precipitation*

Figure 4 presents CP-2 measurements along a vertical section through a rapidly developing convective cell (at 54-km range) observed near Huntsville, Alabama, on 25 July 1986. Approximately 20–25 min after development of a “first echo,” the cell contains a peak  $Z_h$  core at 5 km AGL exceeding 50 dBZ (Fig. 4a).

Measurements of  $Z_{DR}$  in the cell shown in Fig. 4b clearly delineate the region of ice precipitation aloft ( $Z_{DR}$  near 0 dB) from the rain below ( $Z_{DR}$  2–4 dB). These data, however, also show that large raindrops are present in the precipitation core well above the 0°C level at 5 km AGL. In contrast, raindrops are found only below the 0°C level in the dissipating cell seen between 60- and 70-km range. The persistence of raindrops above the 0°C level throughout the growth stage of the developing cell is direct evidence of the importance of the raindrop coalescence process in convec-

***The persistence of raindrops above the 0°C level throughout the growth stage of the developing cell is direct evidence of the importance of the raindrop coalescence process in convective precipitation development in this region of the United States.***

tive precipitation development in this region of the United States. Observations by Illingworth et al. (1987), Caylor and Illingworth (1987), and Illingworth (1988) yield similar evidence of coalescence growth in convective cells observed in Great Britain.

The LDR measurements shown in Fig. 4c reveal unique information about the structure of precipitation in the developing cell. LDR values in the rain below 5 km AGL and in the solid precipitation near echo top are quite low (–27 to –29 dB), which is consistent with the values observed outside the hail shaft in Fig. 4. A marked signature of high LDR (–20 to –16 dB), however, is seen to sit atop or slightly straddle the boundary between liquid and solid precipitation identified in Fig. 4b. As this boundary changed in position during the growth and decay stages of the cell, the position of the high LDR signature closely followed.

The position and behavior of the LDR signature in Fig. 4c suggests that it marks a region of tumbling, solid precipitation in wet growth. The solid precipitation may either be graupel or frozen drops. In either case, however, water coating serves to raise the depolarization to the level observed, and such a water

coating could easily result from encounter with unfrozen drops. Further study of this and similar cases is in progress, and these studies are expected to better define the promising role that LDR measurements can play in monitoring the evolution of mixed-phase conditions in cloud.

### *c. Mature convective precipitation*

Figure 5 presents CP-2 measurements along a vertical section at 145° azimuth through a severe hailstorm observed near Denver, Colorado, on 13 June 1984. Blanchard and Howard (1986) present an overview of the structure and life cycle of this storm, which caused approximately \$350 million in damage, primarily due to hailfall in the Denver area.

The  $Z_h$  structure shown in Fig. 5a reveals peak reflectivities of 63–65 dBZ in the convective core at 22-km range. Weaker anvil precipitation is present aloft beyond 30-km range, although evaporation below 4 km AGL prevents most of this precipitation from reaching the ground. A weak radar bright band is visible inside 10-km range and indicates that the melting level is at about 3 km AGL. The storm inflow region beyond 23-km range is marked by an echo-weak vault.

The  $Z_{DR}$  data shown above the melting level in Fig. 5b are closely distributed around mean values of –0.1 to 0.4 dB, indicating that the precipitation was in the form of ice rather than raindrops. The increase in  $Z_{DR}$  of 0.2 to 0.3 dB seen beyond 25-km range is a weak indication that the particles in the anvil region presented a slightly more oblate cross section than those falling closer to the precipitation core. This increase in  $Z_{DR}$  with range is inconsistent with the effects of differential attenuation, which would induce a slight decrease in  $Z_{DR}$ . Rain is clearly indicated by the higher values of  $Z_{DR}$  seen beneath the melting level out to 20-km range.

The high values of  $Z_h$  and near-zero values of  $Z_{DR}$  seen in the precipitation core at the surface (22-km range) constitute a well-defined  $Z_{DR}$  hail signature (Bringi et al. 1984) and indicate that hail reached the surface at this location. An echo-weak vault marks the inflow region of the storm, just beyond the precipitation core at the surface. The high values of  $Z_{DR}$  shown at 2–3 km AGL in the storm inflow region (23–29-km range) are indicative of supercooled water drops several millimeters in diameter. This indication of large drops carried via storm inflow is suggestive of the recirculation mechanism first proposed by Browning and Foote (1976), in which raindrops that are carried into the updraft at low levels freeze and become the embryos of hailstones.

Observations of LDR for the same vertical section reveal interesting substructure in the precipitation (Fig. 5c). As seen in the earlier stratiform case, LDR in

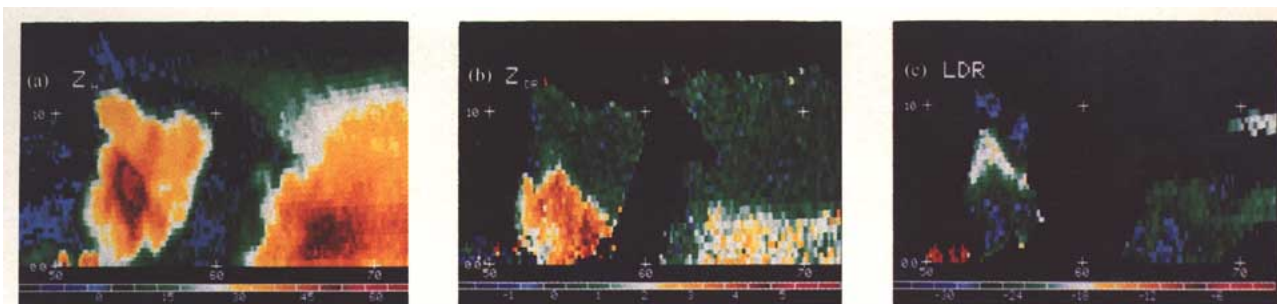


FIG. 4. As in Fig. 3, but for a rapidly developing convective cell (at 54-km range) observed near Huntsville, Alabama, on 25 July 1986. Color scales at bottom of (a), (b), and (c) indicate values of  $Z_h$ ,  $Z_{DR}$ , and LDR, respectively. Evidence of supercooled water drops above the 5-km freezing level is given in (b). LDR signature associated with mixed-phase precipitation growth is given in (c).

the light solid and liquid precipitation observed inside 15-km range is quite low,  $-26$  to  $-29$  dB. An LDR bright band is clearly visible in the melting region. High values of LDR ( $-18$  to  $-10$  dB) are found in the precipitation core, indicating that large, tumbling, nonspherical particles such as irregular hail or graupel are present. Since particle wetting enhances the depolarizing effects of solid precipitation, one might speculate that the very high values of LDR found in the precipitation core are suggestive of particles bearing a water coat in a mixed-phase environment.

The LDR data in Fig. 5c also provide clear evidence of strong propagation effects. In the rain region, LDR increases steadily beyond 12-km range. This behavior is consistent with the influence of differential attenuation and differential phase shift, which are to be expected in propagation through heavy rain. LDR increases further in propagation through the surface hail shaft at 22-km range and fails to return to low values in the low- $Z_h$  region beyond the hail shaft. Thus, it appears that the radar signal was severely corrupted by propagation through the hail shaft. Similar (though less dramatic) effects can be seen to result from propagation through the ice-phase anvil precipitation and the core aloft. Although the physical processes

responsible for the propagation effects observed in the ice-phase precipitation are not fully understood, Herzegh and Jameson (1989) suggest that they result from changes in the polarization state of the propagating wave, as discussed in section 2c.

#### d. Comparison with dual-wavelength observations

Signs such as high reflectivity, a prominent  $Z_{DR}$  hail signature, and surface hail observations leave no question that hail was produced in the precipitation core shown in Fig. 5. Since high values of LDR result from particle characteristics such as asymmetric shape, canted orientations, and particle wetting, it is not surprising that the lower region of the precipitation core, which is known to have contained hail, also had the maximum LDR values observed (Fig. 5c). The vertical continuity of this high-LDR signature suggests that hail content (for the azimuth shown in Fig. 5) extended through a narrow zone to near 9 km AGL. Although direct confirmation of this indication is not possible, strong supporting evidence can be derived from dual-wavelength radar observations, which can be used for hail detection as described below.

Hail can behave like a Rayleigh-Gans scatterer having a strong size dependence at long radar wave-

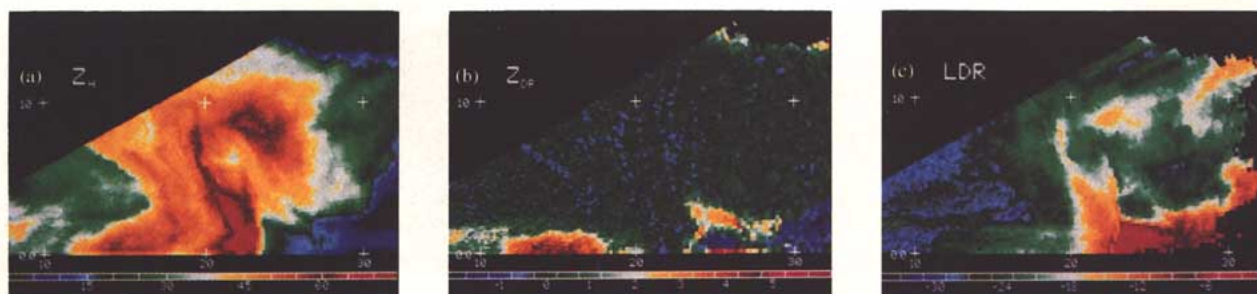


FIG. 5. As in Fig. 3, except for a severe hailstorm observed over Denver, Colorado, on 13 June 1984. Color scales at bottom of (a), (b), and (c) indicate values of  $Z_h$ ,  $Z_{DR}$ , and LDR, respectively. (a)  $Z_h$  (dBZ), showing the precipitation core at 22-km range. (b)  $Z_{DR}$  (dB), showing a hail signature at the surface at 22-km range and a region of supercooled water drops in the storm inflow aloft from 23- to 29-km range. (c) LDR (dB), showing significant propagation effects through the rain near the surface and beyond the precipitation core aloft.

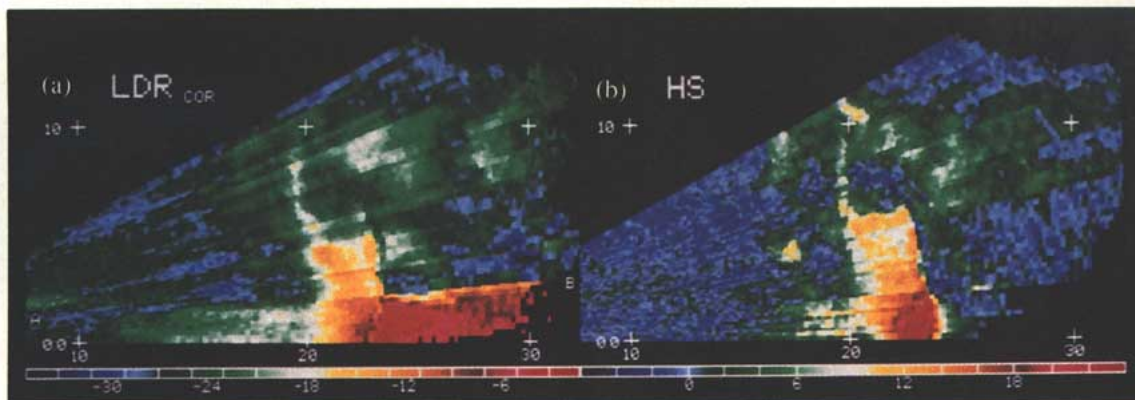


Fig. 6. CP-2 measurements for the vertical section shown in Fig. 5. Color scales at bottom of (a) and (b) indicate values of LDR and the dual-wavelength hail signal (HS), respectively. (a) LDR in decibels. Region above line AB has been corrected to remove propagation effects as noted in section 2c. Region below line AB contains uncorrected data strongly corrupted by propagation effects beyond 12-km range. (b) Dual-wavelength HS in decibels. Note correspondence between high values of LDR and strong hail signal.

lengths (for example, 10 cm) and a Mie scatterer with a weaker, variable dependence on size at short wavelengths (for example, 3 cm). Recognizing this, Atlas and Ludlam (1961) proposed that the ratio of simultaneous measurements of backscattered power at different wavelengths could be used to locate hail. This idea was refined to account for the presence of attenuation at the short wavelength (Jameson 1977; Eccles 1979; Tuttle and Rinehart 1983).

Simply put, the dual-wavelength hail signal (HS) is equivalent to the quantity  $Z_{10}$  minus  $Z_3$ , where  $Z_{10}$  is the measured radar reflectivity (in dBZ) at 10-cm wavelength, and  $Z_3$  (in dBZ) is the radar reflectivity (corrected for attenuation) at 3-cm wavelength. Rain and solid precipitation less than about 1 cm in diameter behave like Rayleigh-Gans scatterers. Thus,  $Z_{10}$  and  $Z_3$  are equal for particles of this size, leading to an HS of  $\sim 0$  dB. However, at 3-cm wavelength, larger precipitation particles behave like Mie scatterers. Thus, these scatterers yield lower measured reflectivities at 3-cm than at 10-cm wavelength, leading to a positive hail signal of several decibels or more. Due to random fluctuation in the returned power at both wavelengths and other uncertainties, values of HS less than about 6 dB are likely to contain a significant fraction of "false" hail indications. Thus, it is common practice to ignore such weak hail signals.

The dual-wavelength hail signal values shown in Fig. 6b bear a remarkably close relation to the propagation-corrected LDR measurements shown in Fig. 6a. Hail signal values are 6 dB or more in the precipitation core below about 6 km AGL, where LDR values exceed  $-18$  dB. In addition, strong hail signals are found in the smaller regions above 6 km, which are marked by similar LDR values. Thus, the suggestion

that the high LDR values observed aloft in the cell correspond to regions of hail is qualitatively confirmed in this case by independent dual-wavelength observations.

The hail signal values in Fig. 6b become very large ( $> 24$  dB) near the back of the precipitation shaft below 2 km AGL. This maximum is an artifact of the dual-wavelength technique and does not relate directly to the hail present at that location. The artifact results from underestimating the attenuation of the 3-cm signal in the very heavy rain in and near the precipitation core. As discussed by Jameson and Heymsfield (1980), inaccuracies in the estimates of attenuation are likely when little backscattered return is received from regions just beyond a precipitation shaft. In the present case, this factor is only significant for observations below the  $0^\circ\text{C}$  level, where heavy rain yielded strong attenuation.

The hail signal and corresponding LDR measurements obtained along the ray path shown in Fig. 7 suggest a strong correlation between these two parameters in the case examined. It is important to note, however, that these two measurement techniques are quite different in nature. While the dual-wavelength hail signal responds to hydrometeor size, high values of LDR result from particle characteristics such as asymmetric shape, canted orientations, and particle wetting. As a result, there are clearly defined conditions in which the correlation apparent in Fig. 7 will break down. For example, in hail that is nearly spherical, LDR values will be very low, even if the stones are tumbling. On the other hand, canted or tumbling nonspherical graupel particles less than  $\sim 1$  cm in diameter will not produce a dual-wavelength hail signal, but are likely to yield relatively high values of LDR.

Thus, the anomalies between hail signal and high values of LDR in Fig. 6 are likely to be a reflection of the fundamental difference in the origins of the two fields. Both quantities, however, contribute significantly to the probing of precipitation characteristics.

#### 4. Summary and discussion

The brief examples discussed above indicate that simple examination of the copolar quantity  $Z_{DR}$  and the cross-polar quantity LDR can reveal key characteristics of precipitation type. In convective systems,  $Z_{DR}$  can provide the information needed to detect regions of liquid precipitation above the 0°C level. This is now finding use in defining the physical processes responsible for the initial formation of precipitation in convective clouds (Illingworth 1988). Measurements of  $Z_{DR}$  may also play a central role in differentiating among solid ice forms such as hail, aggregate snow, and single-crystal snow. Quantitative application of  $Z_{DR}$  measurements in rainfall estimation and  $Z_{DR}$ -based surface hail-detection algorithms already constitute important operational issues.

LDR observations offer, at present, a qualitative indicator of contrasts in ice-particle shape or orientation and particle phase. These responses are seen to be particularly relevant to the delineation of mixed-phase regions aloft and the discrimination of hail from other solid precipitation forms. Further study holds promise for reducing the ambiguity in interpretation of LDR measurements and in defining the methodology for application of LDR data to quantitative estimates of

hail size and density. The marked LDR propagation effects discussed in sections 2c and 3c tend to be enhanced at wavelengths < 10 cm, and call attention to the need to examine the wavelength at which dual-polarization measurements are obtained, particularly for observations in moderate to heavy precipitation.

While a number of significant inferences can be made from  $Z_{DR}$ , LDR, and  $Z_h$  observations alone, the full impact of dual-polarization measurements will not be realized until analyses include a more complete set of simultaneous multiparameter radar observations. At a minimum, this should include observations of Doppler velocity, attenuation, differential phase shift, and signal correlation statistics. To date, there have been few opportunities to examine the interrelationships among these parameters in well-documented meteorological situations. Thus, conduct of comprehensive field experiments incorporating a broad spectrum of multiparameter radar observables and in situ air- and ground-truth measurements represents a high priority for future research. While such studies are of intrinsic scientific interest, a fully developed capability for interpretation of polarization measurements promises greater understanding of precipitation evolution, its interaction with dynamics, and its effects on cloud radiative properties.

*Acknowledgments.* Partial support for data collection and analysis by PHH was provided by the U.S. Army Research Office. Support for ARJ was provided by the National Science Foundation through Grant ATM-86-01257. The authors thank the staff of NCAR's Remote Sensing Facility for their dedicated efforts in collecting the CP-2 data.

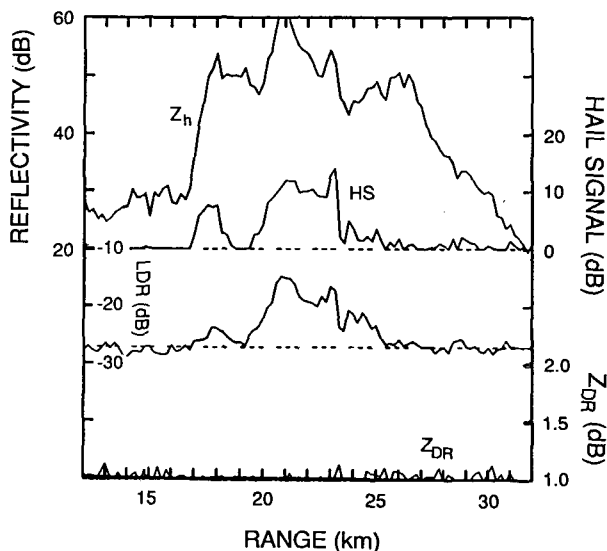


FIG. 7. Line plots of  $Z_h$ , HS, LDR, and  $Z_{DR}$  measured by the CP-2 radar along a ray through the 13 June 1984 hailstorm.

#### References

- Atlas, D., Ed., 1990: *Radar in Meteorology*. Amer. Meteor. Soc., 806 pp.
- , and F.H. Ludlam, 1961: Multi-wavelength radar reflectivity of hailstorms. *Quart. J. Roy. Meteor. Soc.*, **87**, 523–534.
- Aydin, K., T.A. Seliga, and B. Balaji, 1986: Remote sensing of hail with a dual linear polarization radar. *J. Climate Appl. Meteor.*, **25**, 1475–1484.
- Bader, M.J., S.A. Clough, and G.P. Cox, 1987: Aircraft and dual polarization radar observations of hydrometeors in light stratiform precipitation. *Quart. J. Roy. Meteor. Soc.*, **113**, 491–515.
- Battan, L. J., 1973: *Radar Observation of the Atmosphere*. University of Chicago Press, 324 pp.
- Beard, D.V., and D. Chuang, 1987: A new model for the equilibrium shape of raindrops. *J. Atmos. Sci.*, **44**, 1509–1524.
- Beard, K.V., and A.F. Jameson, 1983: Raindrop canting. *J. Atmos. Sci.*, **40**, 448–454.
- Blanchard, D.O., and K.W. Howard, 1986: The Denver hailstorm of 13 June 1984. *Bull. Amer. Meteor. Soc.*, **67**, 1123–1161.
- Bringi, V.N., T.A. Seliga, and K. Aydin, 1984: Hail detection with a differential reflectivity radar. *Science*, **225**, 1145–1147.
- , J. Vivekanandan, and J.D. Tuttle, 1986: Multiparameter radar measurements in Colorado convective storms. Part II: Hail detection. *J. Atmos. Sci.*, **43**, 2564–2577.

- Browning, K.A., and G.B. Foote, 1976: Airflow and hail growth in supercell storms and some implications for hail suppression. *Quart. J. Roy. Meteor. Soc.*, **102**, 499–533.
- Caylor, I.C., and A.J. Illingworth, 1987: Radar observations and modelling of warm rain initiation. *Quart. J. Roy. Meteor. Soc.*, **113**, 1171–1191.
- Eccles, P.J., 1979: Comparison of remote measurements by single and dual-wavelength meteorological radars. *IEEE Trans. Geophys. Electron.*, **17**, 205–218.
- Gans, R., 1912: Über die Form ultramikroskopischer Goldteilchen. *Ann. Phys.*, **37**, 881–900.
- Hall, M.P.M., S.M. Cherry, J.W.F. Goddard, and G.R. Kennedy, 1980: Raindrop sizes and rainfall rate measured by dual polarization radar. *Nature*, **285**, 195–198.
- , J.W.F. Goddard, and S.M. Cherry, 1984: Identification of hydrometeors and other targets by dual-polarization radar. *Radio Sci.*, **19**, 132–140.
- Hendry, A., and Y.M.M. Antar, 1984: Precipitation particle identification with centimeter wavelength dual-polarization radars. *Radio Sci.*, **19**, 115–122.
- , —, and G.C. McCormick, 1987: On the relationship between the degree of preferred orientation in precipitation and dual-polarization radar echo characteristics. *Radio Sci.*, **22**, 37–50.
- Herzogh, P.H., and R.E. Carbone, 1984: The influence of antenna illumination function characteristics on differential reflectivity measurements. Preprints, *22d Radar Meteor. Conf.*, Zurich, Switzerland, Amer. Meteor. Soc., 281–286.
- , and A.R. Jameson, 1989: Dual-polarization radar observations of precipitation: Propagation effects at linear polarization in ice. Preprints, *24th Radar Meteorology Conf.*, Tallahassee, Florida, Amer. Meteor. Soc., 315–317.
- Humphries, R.G., 1974: Observations and calculations of depolarization effects at 3 GHz due to precipitation. *J. Rech. Atmos.*, **8**, 155–161.
- Illingworth, A.J., 1988: The formation of rain in convective clouds. *Nature*, **336**, 754–756.
- , and I.J. Caylor, 1988: Identification of precipitation using dual polarization radar. *Proc. Cloud Physics Conf.*, Bad Homburg, Fed. Rep. of Germany, 372–377.
- , J.W.F. Goddard, and S.M. Cherry, 1986: Detection of hail by dual-polarization radar. *Nature*, **320**, 431–433.
- , —, and —, 1987: Polarization radar studies of precipitation development in convective storms. *Quart. J. Roy. Meteor. Soc.*, **113**, 469–489.
- Jameson, A.R., 1977: A dual-wavelength radar study of a hailstorm, Ph.D. Dissertation, Dept. Geophys. Sci., University of Chicago, 179 pp.
- , 1983: Microphysical interpretation of multi-parameter radar measurements in rain. Part II: Estimation of raindrop distribution parameters by combined dual-wavelength and polarization measurements. *J. Atmos. Sci.*, **40**, 1803–1813.
- , 1985: On deducing the microphysical character of precipitation from multiple-parameter radar polarization measurements. *J. Climate Appl. Meteor.*, **24**, 1037–1047.
- , 1987: Relations among linear and circular polarization parameters measured in canted hydrometeors. *J. Atmos. Oceanic Technol.*, **4**, 634–645.
- , and A.J. Heymsfield, 1980: Hail growth mechanisms in a Colorado storm. Part I: Dual-wavelength radar observations. *J. Atmos. Sci.*, **37**, 1763–1778.
- , and J.H. Davé, 1988: An interpretation of circular polarization measurements affected by propagation differential phase shift. *J. Atmos. Oceanic Technol.*, **5**, 405–415.
- Jayaweera, K.O.L.F., and B.J. Mason, 1965: The behavior of freely-falling cylinders and cones in a viscous fluid. *J. Fluid Mech.*, **22**, 709–725.
- , and R.E. Cottis, 1969: Fall velocities of plate-like and columnar ice crystals. *Quart. J. Roy. Meteor. Soc.*, **95**, 703–709.
- Johnson, D.B., and K.V. Beard, 1984: Oscillation energies of colliding raindrops. *J. Atmos. Sci.*, **41**, 1235–1241.
- Keeler, R.J., B.W. Lewis, and G.R. Gray, 1989: Description of NCAR/FOF CP-2 meteorological Doppler radar. Preprints, *24th Radar Meteorology Conf.*, Tallahassee, Florida, Amer. Meteor. Soc., 589–592.
- Knight, C.A., and N.C. Knight, 1970: The falling behavior of hailstones. *J. Atmos. Sci.*, **27**, 672–681.
- List, R., and R.S. Schemenauer, 1971: Free-fall behavior of planar snow crystals, conical graupel and small hail. *J. Atmos. Sci.*, **28**, 110–115.
- , U.W. Rentsch, and A.C. Byram, 1973: On the aerodynamics of spheroidal hailstone models. *J. Atmos. Sci.*, **30**, 653–661.
- Liu, J.-L., and P.H. Herzogh, 1986: Observations of precipitation particle type by aircraft and dual-polarization radar. Preprints, *23rd Radar Meteorology Conf.*, Snowmass, Colorado, Amer. Meteor. Soc., 59–61.
- McCormick, G.C., and A. Hendry, 1974: Polarization properties of transmission through precipitation over a communication link. *J. Rech. Atmos.*, **8**, 175–187.
- Metcalf, J.I., 1986: Interpretation of the auto-covariances and cross-covariances from a polarization diversity radar. *J. Atmos. Sci.*, **43**, 2479–2498.
- Podzimek, J., 1965: Movement of ice particles in the atmosphere. *Proc. Cloud Physics Conf.*, Tokyo-Sapporo, Meteor. Soc. Japan, 224–230.
- , 1968: Aerodynamic conditions of ice crystal aggregation. *Proc. Cloud Physics Conf.*, Toronto, Amer. Meteor. Soc., 295–298.
- Pruppacher, H.R., and K.V. Beard, 1970: A wind tunnel investigation of the internal circulation and shape of water drops falling at terminal velocity in air. *Quart. J. Roy. Meteor. Soc.*, **96**, 247–256.
- Sachidananda, M., and D.S. Zrnić, 1986: Differential propagation phase shift and rainfall rate estimation. *Radio Sci.*, **21**, 235–257.
- Seliga, T.A., and V.N. Bringi, 1976: Potential use of radar differential reflectivity measurements at orthogonal polarizations for measuring precipitation. *J. Appl. Meteor.*, **15**, 69–76.
- , —, and H.H. Al-Khatib, 1981: A preliminary study of comparative measurements of rainfall rate using the differential reflectivity technique and a raingage network. *J. Appl. Meteor.*, **20**, 1362–1368.
- Tuttle, J.D., and R.E. Rinehart, 1983: Attenuation correction in dual-wavelength analyses. *J. Climate Appl. Meteor.*, **22**, 1914–1921.
- Ulbrich, C.W., and D. Atlas, 1984: Assessment of the contribution of differential polarization to improved rainfall measurements. *Radio Sci.*, **19**, 49–57.
- Zikmunda, J., and G. Vali, 1972: Fall patterns and fall velocities of rimed ice crystals. *J. Atmos. Sci.*, **29**, 1334–1347.